Power-law scaling in human EEG:

Relation to Fourier power spectrum

*T. C. Ferree[1] and R. C. Hwa[2]

[1] Dynamic Neuroimaging Laboratory, Department of Radiology, University of California San Francisco

[2] Institute of Theoretical Science and Department of Physics, University of Oregon

February 7, 2002

Abstract

It has recently been demonstrated that human EEG time series exhibit power-law scaling behavior typically over two temporal regions. The scaling exponents provide a concise description of the complex nonlinear fluctuations without assuming low-dimensional chaotic attractors. This paper illustrates the concept, and compares the results to the Fourier power spectrum for real data. It also presents a simple algorithm for optimally fitting scaling exponents, while at the same time quantifying the quality of the scaling behavior. A companion paper [7] discusses fluctuations across multiple electrodes, and an application to clinical stroke detection.

Keywords: Electroencephalography, power-law, scaling, fractal, complexity.

PREPRINT

Submitted to 2002 Computational Neuroscience Meeting

*Corresponding author. Telephone: (415) 502-3726; Email: tom.ferree@radiology.ucsf.edu

1 Introduction

The brain is obviously a complex system, and exhibits rich spatiotemporal dynamics. Among the noninvasive techniques for human research and clinical diagnosis, scalp electroencephalography (EEG) provides a direct measure of brain electrical activity with millisecond temporal resolution [10]. A major challenge facing neuroscientists is how to effectively characterize the complex patterns so measured. New statistical measures provide new opportunities for relating EEG signals to brain function and pathology.

The most commonly used techniques for analyzing EEG time series are still very simple. For identifying event-related activity, post-stimulus- or post-response-time ensemble averaging give an estimate of the impulse response function [4]. For quantifying ongoing (resting) EEG, the Fourier power spectrum decomposes the signal in terms of sinusoidal oscillations [15]. Both of these techniques originate in linear systems theory. Chaos theory has also been applied to study nonlinear behavior [3]. In several examples, e.g., epileptic seizure [1], low-dimensional chaotic dynamics have been observed. Nevertheless, it has slowly become appreciated that chaos theory is not entirely satisfactory for quantifying brain dynamics, because it assumes the existence of low-dimensional attractors not always manifest by high-dimensional complex systems [12].

We describe here an alternative approach which avoids the assumptions of linearity and low-dimensional chaotic attractors, and gives a measure of EEG temporal fluctuations *across a range of temporal scales*. The approach is aimed at identifying power-law scaling behavior, nearly ubiquitous in complex systems [2]. Complex systems usually exhibit fluctuations across of broad range of time scales, and it is of interest to quantify this behavior. For a system to exhibit power-law scaling behavior means that the fluctuations $F(k)$, computed on a scale k, obey the relation

$$F(k) \propto k^{\alpha} \ . \tag{1}$$

If this expression holds, then the scaling exponent α provides a succinct measure of the dynamics across a range of time scales. For geometric fractals, such behavior persists without limit, while for physical systems it may be interrupted by dynamical mechanisms which introduce a characteristic

time scale, but may still hold over limited ranges.

In this paper, we show examples of resting EEG data which exhibit power-law scaling behavior over two temporal regions. We also compute the Fourier power spectra and discuss the similarities and differences. Finally, based on careful error analysis of the fluctuation measure $F(k)$, we provide a simple algorithm for optimally fitting the scaling exponents over two temporal regions. This provides two additional measures of the EEG dynamics which may also prove informative.

2 Power-law scaling behavior

To quantify the EEG fluctuations, we use the technique of detrended fluctutation analysis (DFA), first invented to study long-range correlations in nucleotide sequences [13], then adapted to study long-range correlations in the heart interbeat intervals [14]. DFA has been applied to wavelet-filtered EEG to study long-range correlations in α-band oscillations [8], and to unfiltered EEG by our group [5, 6]. The detrending renders the method relatively insensitive to nonstationarities in the data.

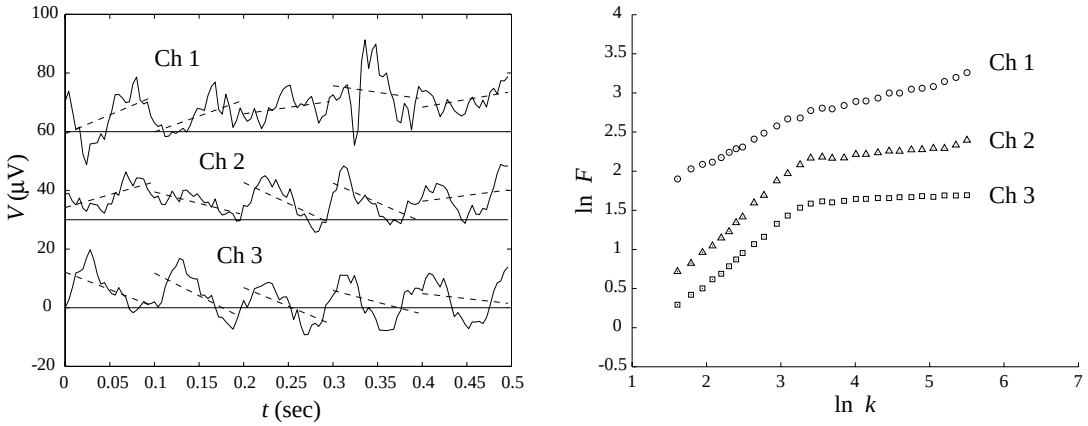

Figure 1: (a) Examples of EEG time series in three channels for a single subject. The vertical scales of Ch. 1 and Ch. 2 are shifted upward by 60 and 30 μV, respectively. Dashed lines indicate semi-local trends for $k = 25$. (b) $\ln F(k)$ versus $\ln k$ for the three channels in (a). The vertical scales of Ch. 1 and Ch. 2 are shifted upward by 1.0 and 0.5 units, respectively. Errors in $\ln F(k)$ are shown with vertical lines (mostly appearing as dots) inside plot symbols (see Section 3).

To define $F(k)$, let an EEG time series be denoted by $V(t)$, where t is discrete time ranging from 1 to T. Divide the entire range of t to be investigated into B equal windows, discarding any remainder, so that each window has $k = \mathrm{floor}(T/B)$ time points. Within each window, labeled b ($b = 1, \ldots, B$), perform a least-square fit of $V(t)$ by a straight line, $\overline{V}_b(t)$, i.e., $\overline{V}_b(t) = \mathrm{Linear\text{-}fit}[V(t)]$ for $(b-1)k < t \leq bk$. That is the semi-local trend for the bth window. The squared fluctuation from the semi-local trend in the bth window is defined

$$F_b^2(k) = \frac{1}{k} \sum_{t=1+(b-1)k}^{k+(b-1)k} [\, V(t) - \overline{V}_b(t) \,]^2 \ . \tag{2}$$

This quantity is averaged over B windows to yield

$$F(k) = \sqrt{\frac{1}{B} \sum_{b=1}^{B} F_b^2(k)} \ . \tag{3}$$

$F(k)$ is a measure of the fluctuations in each window averaged over B windows, and is also the RMS fluctuation from the semi-local trends concatinated over B windows each having k time points. Equation (1) implies $\ln F(k) \propto \alpha \ln k$, thus linear regions in plots of $\ln F(k)$ versus $\ln k$ indicate power-law behavior, with the slope of the line giving the exponent α. Using DFA to quantify the fluctuations provides a useful theoretical limit. An uncorrelated random walk gives $\alpha = 1/2$ identically [9], while other values of α give a measure of temporal correlations.

Figure 1a shows the first 0.5 sec of three 10-second EEG times series for a normal subject, resting with eyes closed. The data were hardware filtered between 0.1 Hz and 100 Hz, and digitized at 250 Hz. The semi-local trends $\overline{V}_b(t)$ are shown as dashed lines. Figure 1b shows log-log plots of $F(k)$ versus k for the three channels in Fig. 1a, for values of k from 5 to 250, in approximately equal steps of $\ln k$. For each channel shown, it is evident that power-law behavior exists over two temporal regions. We have analyzed 128 EEG time series for each of 18 normal subjects [6], and found similar scaling behavior in nearly all cases. This is a remarkably simple behavior for such complex data sets, and provides a heretofore unrecognized approach for characterizing brain dynamics.

3 Relation to Fourier power spectrum

By far the most common method of analyzing resting EEG time series is the Fourier transform. The power spectrum is computed as a function of frequency and usually the emphasis is placed on individual peaks which indicate particular characteristic frequencies. This is very different than scaling analysis, which emphasizes relationships *across* time scales. It is also widely noted, however, that the power spectrum of many complex systems, including the EEG, exhibits "$1/f^{\beta}$" behavior at low frequencies. Thinking of the power spectrum this way is a form of scaling analysis, but one which still relies upon decomposing the signal into a linear superposition of sine waves.

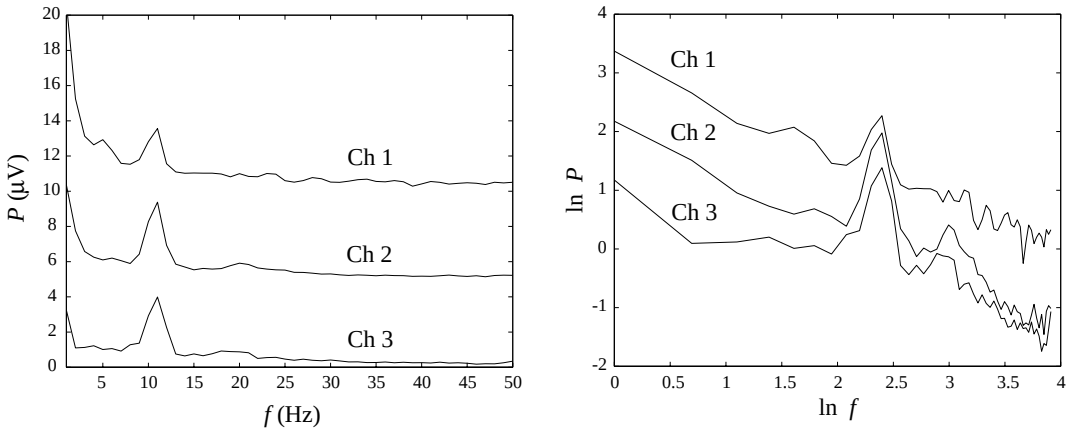

Figure 2: Fourier transform of the three time series in Fig. 1a. (a) Linear axes. The vertical scales of Ch. 1 and Ch. 2 are shifted upward by 10 and 5 μV, respectively. (b) Log-Log coordinates. The vertical scales of Ch. 1 and Ch. 2 are shifted upward by 1 and 0.5 units, respectively.

We computed the Fourier power spectrum for the three time series in Fig. 1a. Each 10-second data segment was divided into ten 1-second segments. Each 1-second segment was Hann windowed, then Fourier transformed using a standard FFT algorithm. This gives 1 Hz frequency resolution. The Fourier amplitude P was computed by taking the complex modulus, normalizing for the effects of windowing, then averaging over the ten 1-second segments. Figure 2a shows P plotted on linear-linear axes. A clear peak is evident near 10 Hz. Figure 2b shows P plotted on log-log axes. The peak near 10 Hz is still evident. At frequencies below the peak, $\ln P$ falls with $\ln f$, although not monotonically. At frequencies above the peak, the behavior is completely erratic. Clearly the DFA

behavior in Fig. 1b is much more amenable to description with a few parameters.

We have compared the results of Fourier and DFA analysis for the 18 subjects in Ref. [6], plus 10 subjects suffering from acute ischemic stroke [7]. The following observations are made: (1) In the $\ln P$ vs $\ln f$ plots, we see a general tendency for $\ln P$ to decrease with $\ln f$, except for the giant peak near $f = 10$ Hz that dominates the landscape in all channels; (2) The frequency of the dominant peak in $\ln P$ can be related to the value of k at which the bend occurs in Fig. 1b; (3) The behavior of $\ln F$ is always much smoother than $\ln P$, especially at shorter time scales (higher frequencies), making it amenable to concise summary with a small number of parameters. This last feature is particularly advantageous when the objective is to consider 128 channels across many subjects.

4 Optimal fitting

To capture the essence of the scaling behavior in Fig. 1b, there are multiple ways to fit the scaling exponents α_1 and α_2. The simplest is to define two regions (e.g., Region 1: $1 < \ln k < 2.5$; Region 2: $3.5 < \ln k < 5.75$) which are well separated from the location of the bend [5, 6]. This has the virtue of capturing the behavior in each region reasonably well, even when the bend is not sharp, as is occasionally the case. When the bend is sharp, a better approach is to optimally fit two lines, while considering the location of the bend a free parameter, and accept the lines which minimize the overall fitting error. We develop this approach here.

Optimally fitting lines to the curves in Fig. 1b requires estimates of the errors in $\ln F(k)$. There are three main sources of error in the original voltage data $V(t)$. First, the EEG amplifiers introduce to each time point a Gaussian random variable with RMS amplitude 0.6 μV. Second, there is often a slow drift associated with changing quality of scalp-electrode contact, but fortuitously this tends to be removed by the detrending in DFA. Third, approximation of potentials relative to infinity via the average reference [10], used here, or any technique for deconvolving scalp potentials to the brain surface, introduces further errors in the signal to be analyzed. To illustrate the procedure here, we consider only errors due to amplifier noise. In accordance with data, we assume amplifier noise is stationary and normally distributed, with RMS amplitude denoted by $\delta V = 0.6$ μV.

In each window b, the local linear trend $\overline{V}_b(t) = a_b + m_b t$ is obtained using standard techniques in linear regression [11]. Along with the maximum likelihood parameters of the line (a_b, m_b), errors in these parameters $(\delta a_b, \delta m_b)$ are also obtained. Each of these contributions must be accounted for when computing $F(k)$. To do this, we first define an array containing the complete list of quantities on which $F(k)$ depends: $\{r_j\} = \{V_b(t), \{a_b\}, \{m_b\}\}$, where $j = 1, \ldots, kB + 2B$, and consider $F(k) = F(k; \{r_j\})$. Assuming each r_j has a Gaussian random error δr_j, and makes an independent contribution to $F(k; \{r_j\})$, these contributions combine in quadrature according to

$$\delta F(k) = \left[\sum_{j=1}^{(k+2)B} \left(\frac{\partial F}{\partial r_j} \right)^2 \delta r_j^2 \right]^{1/2} . \tag{4}$$

Taking the derivates $\partial F / \partial r_j$ leads to

$$\delta F(k) = \left[\frac{1}{kB} \delta V^2 + \frac{1}{F^2} \frac{1}{B^2} \sum_{b=1}^{B} \left(\left\langle V - \overline{V} \right\rangle_b^2 \delta a_b^2 + \left\langle (V - \overline{V}) \tau \right\rangle_b^2 \delta m_b^2 \right) \right]^{1/2} \tag{5}$$

where $<>_b$ denotes an average over the bth window, and $\tau = (1, \ldots, k)$ is a vector containing the discrete time points in the local coordinates of window b. We allowed the trend errors δa_b^2 and δm_b^2 to depend upon b, since that was found numerically to be the case. To compute the errors in $\ln F(k)$, we trivially compute

$$\delta \ln F(k) = \frac{1}{F(k)} \, \delta F(k) \tag{6}$$

which has the effect of increasing the error $\delta \ln F(k)$ at small values of $F(k)$, i.e., small values of k. This gives the error bars shown in Figure 1b.

To fit the linear behavior in Fig. 1b, we assume there exist two linear regions, which meet at a single point $\ln k = \ln \kappa$. For each value of $\ln \kappa$, we use standard linear regression [11] to compute best-fit lines to the two regions, and sum the χ^2 values. The minimum value of the total χ^2 indicates the best overall fit. Fig. 3a shows the fit error as $E = \sqrt{\chi^2 / \nu}$, where ν is the number of degrees of freedom in the fitting procedure, i.e., the number of points in $\ln \kappa$ minus the number of fitting parameters (equal to four). Figure 3b shows the optimal fits for Chs. 1-3. The slopes of the lines give the scaling exponents α_1 and α_2.

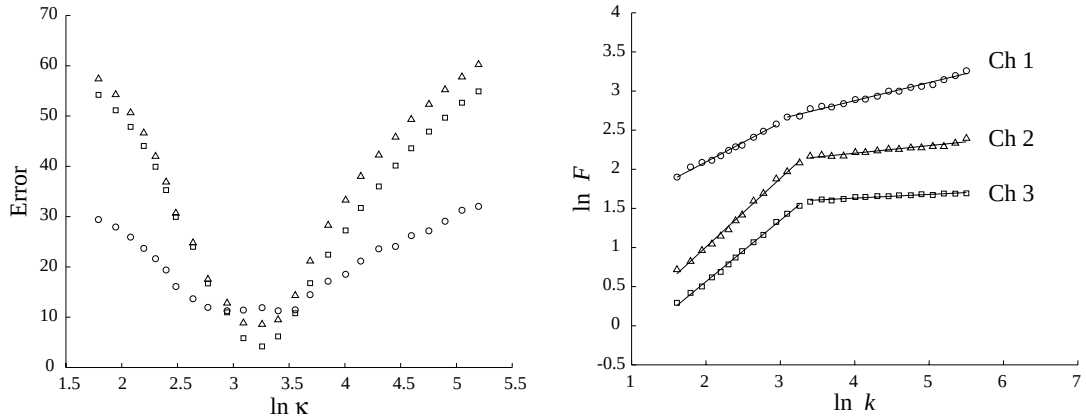

Figure 3: (a) Error measure $E = \sqrt{\chi^2/\nu}$ versus bend location $\ln\kappa$ for Chs. 1-3. (b) Optimal linear fits for Chs. 1-3, with slopes equaling α_1 and α_2. Plot symbols are the same as in Fig. 1b.

The minimum errors for Chs. 1-3 are: 13.2, 8.4 and 5.2, respectively. These values are larger than would be expected for perfect linear behavior. One reason for this is that our estimate of the errors in $\ln F(k)$ are conservative, since they include only amplifier noise. Of course, another reason is that no physical system exhibits perfect power-law scaling behavior. Nevertheless, from a data analysis perspective, the scaling exponents α_1 and α_2 provide a succinct parameterization of the EEG fluctuations *across a range* of temporal scales. The error analysis, beyond supporting an automated algorithm for optimally determining α_1 and α_2, provides two additional measures of the dynamics: 1) a characteristic time scale, given by the bend location κ, and 2) a measure of the "quality" of the scaling behavior, given by the minimum error $E_{\min}$.

5 Discussion

We have discussed how resting EEG time series exhibit power-law scaling behavior typically over two temporal regions. The scaling exponents provide a concise summary of the complex dynamics *across a range of time scales*. We have also demonstrated that the behavior of DFA for quantifing scaling behavior has clear advantages over Fourier analysis, in that DFA is more amenable to concise description with a small number of scaling parameters. This is an advantage for summarizing the

large data sets which arise for 128 channels and many subjects. Finally, we developed a simple algorithm, based upon careful error analysis, for optimally fitting scaling exponents over two temporal ranges.

Compared to Fourier and chaos analysis, scaling analysis has only recently been considered in human EEG. It represents a new paradigm for quantifying the complex, highly nonstationary temporal fluctuations. It remains to be seen what these scaling properties tell us about human brain function and pathology. A companion paper [7] considers the fluctuations over the 128 scalp electrodes, and demonstrates that scaling analysis discriminates remarkably well between normal subjects and those with acute ischemic stroke.

Acknowledgements

We thank Dr. Phan Luu and Prof. Don Tucker for supplying the EEG data for our analysis. We have also benefited from the computational assistance of Wei He. This work was supported, in part, by the National Institutes of Health under Grant Nos. NS-38829 and NS-27900, and by the U.S. Department of Energy under Grant No. DE-FG03-96ER40972.

References

[1] Babloyantz, A. and A. Destexhe (1986). Low dimensional chaos in an instance of epilepsy. Proceedings of the National Academy of Sciences USA 83: 3513-3517.

[2] Bak, P. *How Nature Works: The Science of Self-Organized Criticality.* (Copernicus, 1996).

[3] *Chaos in Brain?* K. Lehnertz, J. Arnhold, P. Grassberger and C. E. Elger (Eds.) (World Scientific, 2000).

[4] Donchin, E. Event-related brain potentials: A tool in the study of human information processing. In: *Evoked Potentials and Behavior.* H. Begleiter, Ed. (New York: Press, 1979).

[5] Hwa, R. C. and T. C. Ferree (2002). Fluctuation analysis of human electroencephalogram. Accepted in: Nonlinear Phenomena in Complex Systems.

[6] Hwa, R. C. and T. C. Ferree (2002). Scaling properties of fluctuations in human electroencephalogram. Submitted to: Physical Review E.

[7] Ferree, T. C. and R. C. Hwa. Power-law scaling in human EEG: Moment analysis and clinical stroke detection. Submitted to: Neurocomputing, this issue.

[8] Linkenkaer-Hansen, K., V. V. Nikouline, J. M. Palva and R. J. Ilmoniemi (2001). Long-range temporal correlations and scaling behavior in human brain oscillations. Journal of Neuroscience 21(4): 1370-1377.

[9] Montroll, E. W. and M. F. Schlesinger. In: *Nonequilibrium Phemonema II: From Stochastics to Hydrodynamics*. J. L. Lebowitz and E. W. Montroll, Eds. (North-Holland, 1984).

[10] Nunez, P. L. *Electric Fields of the Brain*. (Oxford University Press, 1981).

[11] Press, W. H., S. A. Tuekolsky, W. T. Vetterling and B. P. Flannery. *Numerical recipes in C*. Cambridge University Press, 1992).

[12] Palus, M. (1996). Nonlinearity in normal human EEG: cycles, temporal asymmetry, nonstationarity and randomness, not chaos. Biological Cybernetics 75: 389-396.

[13] Peng, C.-K., S. V. Buldyrev, A. L. Goldberger, S. Havlin, F. Sciortino, M. Simons, and H. E. Stanley (1992). Long-range correlations in nucleotide sequences. Nature 356: 168-170.

[14] Peng, C.-K., J. Mietus, J. M Hausdorff, S. Havlin, H. E. Stanley, and . L. Goldberger (1993). Long-range anticorrelation and non-Gaussian behavior of the heartbeat. Physical Review Letters 70(9): 1343-1346.

[15] Walter, D. O. (1963). Spectral analysis for electroencephalograms: Mathematical determination of neurophysiological relationships from records of limited duration. Exp. Neurol. 8: 155-181.